Direct substrate delivery into mitochondrial-fission deficient pancreatic islets rescues insulin secretion

Uma D. Kabra[1,4], Katrin Pfuhlmann[1,4], Adriana Migliorini[1], Susanne Keipert[1], Daniel Lamp[1,4], Olle Korsgren[2], Moritz Gegg[1,4], Stephen C. Woods[5], Paul T. Pfluger[1], Heiko Lickert[1,4], Charles Affourtit[3], Matthias H. Tschöp[1,4] , Martin Jastroch[1 *]

Short running title: Mitochondrial dynamics and insulin secretion

[1]Helmholtz Diabetes Center & German Diabetes Center (DZD), Helmholtz Zentrum München, 85764 Neuherberg, Germany

[2]Department of Immunology, Genetics and Pathology, Uppsala University, Uppsala, Sweden

[3]School of Biomedical and Healthcare Sciences, Plymouth University, Drake Circus, Plymouth PL4 8AA, UK

[4]Division of Metabolic Diseases, Technische Universität München, 80333 Munich, Germany

[5]Department of Psychiatry and Behavioral Neuroscience, University of Cincinnati, Cincinnati OH 45237, USA

[*]Corresponding author:

Martin Jastroch

Helmholtz Diabetes Center & German Diabetes Center (DZD), Helmholtz Zentrum München, 85764 Neuherberg

Institute for Diabetes and Obesity, Parkring 13, D-85748 Garching

Germany

Tel. +49 (0)89 3187 2105

Email martin.jastroch@helmholtz-muenchen.de

Word count: 3971; Figures: 6

Diabetes Publish Ahead of Print, published online February 7, 2017

Abstract

In pancreatic beta cells, mitochondrial bioenergetics control glucose-stimulated insulin secretion (GSIS). Mitochondrial dynamics are generally associated with quality control, maintaining the functionality of bioenergetics. By acute pharmacological inhibition of mitochondrial fission protein *Drp1*, we here demonstrate that mitochondrial fission is necessary for GSIS in mouse and human islets. We confirm that genetic silencing of *Drp1* increases mitochondrial proton leak in MIN6 cells. However, our comprehensive analysis of pancreatic islet bioenergetics reveals that *Drp1* does not control insulin secretion via its effect on proton leak but instead via modulation of glucose-fuelled respiration. Notably, pyruvate fully rescues the impaired insulin secretion of fission-deficient beta cells, demonstrating that defective mitochondrial dynamics solely impact substrate supply upstream of oxidative phosphorylation. The present findings provide novel insights in how mitochondrial dysfunction may cause pancreatic beta cell failure. In addition, the results will stimulate new thinking in the intersecting fields of mitochondrial dynamics and bioenergetics, as treatment of defective dynamics in mitochondrial diseases appears to be possible by improving metabolism upstream of mitochondria.

The development of type-2 diabetes mellitus is associated with mitochondrial dysfunction in pancreatic beta-(β)-cells. β-cells have developed highly coordinated mechanisms that link glucose sensing with metabolic signaling cascades that direct the secretion of sufficient insulin to maintain glucose homeostasis [1]. The mechanism underlying glucose-stimulated insulin secretion (GSIS) from β-cells involves glucose uptake by specific glucose transporters followed by glucose catabolism through glycolysis yielding pyruvate, which in turn is further catabolized via the tricarboxylic (TCA) cycle. Both glycolysis and TCA-cycle turnover generate reducing power that is used by the mitochondrial respiratory chain to produce ATP through oxidative phosphorylation. The resultant increase in the cytosolic ATP/ADP ratio closes ATP-sensitive K^+ (K_{ATP}) channels, thus depolarizing the plasma membrane. Depolarization triggers opening of voltage-gated Ca^{2+} channels, and the influx of Ca^{2+} ions consequently leads to exocytosis of insulin-containing granules from β-cells [2]. This sequence of events illustrates that β-cell mitochondria exert strong control over GSIS [3] as mitochondrial energy-transducing processes dictate how fast and efficiently glucose is converted to ATP. Mitochondrial dysfunction impairs glucose-insulin secretion coupling and ultimately promotes β-cell apoptosis and death, one of the key features of type-2 diabetes (T2D) [4].

Mitochondria are dynamic organelles that are constantly remodeled through the opposing action of fission and fusion proteins [5]. Until recently, the influence of mitochondrial dynamics over energy transduction has been under-appreciated. The continuous changes in mitochondrial morphology are controlled by a group of evolutionarily highly-conserved large GTPases of the dynamin superfamily [5]. Mitochondrial fusion is regulated by mitofusins 1 and 2 (*Mfn1/2*) and optic-atrophy 1

(*Opa1*), whereas mitochondrial fission is regulated by dynamin-related protein 1 (*Drp1*) and fission protein 1 (*Fis1*) [6]. Increasing evidence suggests that a subtle balance between mitochondrial fission and fusion events is crucial for achieving the mitochondrial morphology required for a particular (energetic) function [7-9]. Deficiencies in the proteins regulating mitochondrial dynamics have been associated with several human diseases including dominant Optic Atrophy for *Opa1*, Charcot-Marie-Tooth disease type 2A for *Mfn2*, and developmental defects for *Drp1* [10-12]. Indeed, there is evidence that the pancreatic islets of diabetic patients exhibit swollen and enlarged mitochondria, implying disturbed mitochondrial morphology under diabetic conditions [13].

The GTPase gene *Drp1* is considered pivotal for regulating mitochondrial fission [14]. In response to metabolic demand, *Drp1* translocates from the cytoplasm to the mitochondrial surface where it forms a complex with *Fis1*. Oligomerization of *Drp1* provides the mechanical force required to constrict the mitochondrial membranes and thereby facilitate fission [15]. Recent studies suggest that *Drp1* recruitment involves post-translational modifications including sumoylation, S-nitrosylation, ubiquitination, and phosphorylation [16, 17]. Interestingly, *Drp1* activation under glucolipotoxic conditions in pancreatic β-cells leads to abnormalities in mitochondrial structure and function, followed by activation of pro-apoptotic signaling cascades [18-21]. It has recently been reported that manipulation of mitochondrial morphology by overexpressing dominant-negative *Drp1* (*DN-Drp1*) with erased GTPase activity decreases GSIS in INS-1E insulinoma cells, and this was attributed to increased mitochondrial proton leak [22]. Collectively, these findings emphasize the important role of mitochondrial dynamics in pancreatic β-cell biology, although exact mechanisms have yet to be established firmly.

In the present study, we used genetic and pharmacological inactivation of *Drp1* to assess mechanistically how mitochondrial dynamics control mitochondrial energy transduction and subsequently how this impacts GSIS in MIN6 cells, and human and mouse pancreatic islets. We confirm that genetic silencing of the mitochondrial fission protein *Drp1* by use of lentivirus-mediated shRNA disrupts mitochondrial morphology and impairs GSIS in MIN6 cells. We demonstrate that the decrease of insulin secretion is secondary to a decreased ATP synthesis instead of increased mitochondrial proton leak as suggested previously [22]. We exclude long-term effects on autophagy and mitochondrial quality control by acute pharmacological inactivation of *Drp1* with the mitochondrial division inhibitor (mdivi-1). Mdivi-1 displays identical attenuating effects on GSIS in mouse and human pancreatic islets. Mechanistically, however, comprehensive real-time analysis of cellular respiration reveals that the deficient mitochondrial fragmentation lowers coupling efficiency of oxidative phosphorylation by decreasing glucose-fuelled respiration and not by increasing proton leak. Because *Drp1* inhibition did not change respiratory complex subunit concentrations, we hypothesized that mitochondrial substrate supply may be hampered in fission-deficient pancreatic β-cells. Consistent with this, we reveal that direct supply of exogenous (methyl) pyruvate fully rescues deficits in oxidative phosphorylation, ATP output and GSIS in fission-deficient cells and islets. This discovery of physiologically relevant impairments upstream of oxidative phosphorylation offers therapeutic options for treating mitochondrial-dynamics-related β-cell dysfunction and associated metabolic diseases.

Research Design and Methods

Human and mouse islets - Human islets were provided through the JDRF award 31-2008-416 (ECIT islet for basic research program) and islet experiments were

approved by the Ethical Commission of the Technical University of Munich (Germany). Mouse islets were isolated by collagenase digestion as previously described [23]. For details on islet culturing conditions, refer to supplemental data.

MIN6 cells and viral infection – For details on cell culture and viral conditions refer to supplemental data.

Insulin secretion from islets – Equal-number batches of islets were washed twice with HEPES-balanced Krebs-ringer (KRH) bicarbonate buffer composed of 114 mM NaCl, 4.7 mM KCl, 2.5 mM $CaCl_2$, 1.16 mM $MgSO_4$, 1.2 mM KH_2PO_4, 25.5 mM $NaHCO_3$ and 20 mM HEPES, pH 7.2-7.4, supplemented with 0.2% (w/v) bovine serum albumin (BSA) and 2 mM glucose. The islets were starved in the same buffer with and without 100 μM mdivi-1 for 1 h at 37^0C. Later, starvation buffer was aspirated and islets were incubated in KRH bicarbonate buffer with indicated concentrations of glucose and other secretagogues with and without 100 μM mdivi-1 for 1 h at 37^0C. Thereafter, the supernatants were collected, and centrifuged at 760 g for 5 min for determination of insulin concentration using a mouse ultrasensitive insulin ELISA kit (Alpco). Following the secretion assay, islets were washed twice with Dulbecco's PBS, and ice-cold RIPA lysis buffer was added. Islet homogenates were collected, centrifuged at 12000 g for 10 min and assayed for total insulin content by RIA. For normalization, DNA content was measured using the Quant-it Pico Green DNA assay kit (Invitrogen). Each independent experiment was performed with three technical replicates. Refer to the supplemental data for details on insulin secretion from MIN6 cells.

Cellular bioenergetics - An extracellular flux analyzer XF24 (Seahorse Bioscience) was used to determine oxygen consumption rate (OCR). Cells were seeded into XF24-well plates at a density of 40,000 cells/well in DMEM containing 25 mM

glucose. The cells were washed twice with bicarbonate-free KRH buffer containing 2 mM glucose and starved in the same buffer with and without mdivi-1 for 2 h at 37^0C in a non-CO_2 incubator. After recording basal cellular respiration, cells were treated sequentially with glucose (16.5 mM) and other secretagogues, oligomycin (2 μg/ml), and eventually rotenone/antimycin A (1 and 2 μM, respectively) to correct for non-mitochondrial respiration. Respiration values are presented after correction and normalization with DNA content. The respiratory data were analyzed and interpreted according to [24]. In short, "basal respiration" represents mitochondrial respiration rates at 2 mM glucose, and "ATP linked respiration" represents the respiration rates prior to injection of oligomycin minus oligomycin-insensitive rates. Oligomycin-insensitive rates are labeled "proton leak respiration". The coupling efficiency represents the fraction of respiration used to drive ATP synthesis for each run, calculated as CE = 1- (proton leak/respiration prior to oligomycin-injection).

Islet bioenergetics - Batches of equal numbers of islets were plated into XF24-well islet culture plates and washed twice with bicarbonate-free KRH buffer supplemented with 2 mM glucose. The islets were starved in the same buffer with and without 100 μM mdivi-1 for 1 h at 37^0C in a non-CO_2 incubator. The plate was then placed into the machine (controlled at 37°C) for a 10-min calibration followed by four measurement cycles to record basal cellular respiration. Islets were then treated sequentially with glucose (16.5 mM), oligomycin (10 μg/ml), and a mixture of rotenone/antimycin A (R/A; both 2 μM). Respiration values were calculated by subtracting non-mitochondrial respiration. For normalization, DNA content of the cells was measured.

Intracellular ATP Content - Cells were seeded into white 96-well plates at a density of 10,000 cells/well in DMEM containing 25 mM glucose. Cells were treated

similarly as for the insulin-secretion assay. At the end of experiment, medium was aspirated; cells were washed twice with ice-cold Dulbecco's PBS and ATP content was determined using the Luminescent ATP detection assay kit (Abcam). Results were corrected for DNA content.

Glucose Uptake assay, Western blot analysis and RNA isolation and RT-PCR - For details refer to supplemental data.

Mitochondrial morphology - Mitochondrial morphology was examined in live non-target and *Drp1* KD MIN6 cells stained with 40 nM Mito tracker red FM (Invitrogen) for 30 min. After 3-5 washes, cells were examined using a SP5 confocal microscope (Leica) with 60X objective lens.

Statistical analysis - Data were collected from several independent experiments and results are expressed as means ± SEM. Unpaired 2-tailed student t-tests were used to compare two variables, and one-way ANOVA (with Bonferroni posthoc analysis) was used for multiple comparisons using Graph-Pad prism version 6.0. Statistically significant differences were considered at $p<0.05$ (*), $p<0.01$ (**) and $p<0.001$ (***).

Results

Drp1 knockdown changes mitochondrial morphology and decreases GSIS

MIN6 cells targeted with specific shRNA express ~50% less *Drp1* mRNA (Fig. 1a) and 80% less protein (Fig. 1b) than non-targeted control cells. *Drp1* knockdown (KD) did not affect *Mfn1* or *Opa1* mRNA levels but caused an increase in *Mfn2* mRNA, consistent with the concept that mitochondrial elongation is supported (Fig. 1c). Moreover, fluorescent visualization of the mitochondrial network revealed elongated mitochondria in *Drp1* KD cells; i.e., it demonstrated the expected morphological changes (Fig. 1d, e). Western analysis of representative subunits from all respiratory complexes (gene names are found in Fig. 1f) confirms that *Drp1* KD does not affect

the composition of the mitochondrial electron-transfer chain (Fig. 1f). Equally, *Drp1* KD leaves the insulin content of MIN6 cells unaffected (Fig. 1g), although it lowered Ins2 (not Ins1) mRNA (Fig. 1h).

Basal insulin release at 2 mM glucose was not affected by *Drp1* KD, but insulin secretion at 16.5 mM glucose was significantly decreased (Fig. 2a), strongly implicating mitochondrial dynamics in the control of nutrient-secretion coupling in pancreatic β-cells. *Drp1* KD did not affect insulin secretion mechanisms downstream of mitochondria, as neither KCl- nor glyburide-provoked insulin release was changed (Fig. 2a). In the presence of low glucose levels (2 mM), potassium served to depolarize the plasma membrane while glyburide, a sulfonylurea, specifically closes ATP-dependent potassium channels. These findings strongly suggest that *Drp1* KD decreases GSIS through deleterious effects on glucose catabolism.

***Drp1* knockdown lowers coupling efficiency of oxidative phosphorylation**

Real-time oxidative breakdown of glucose can be followed readily in intact cells by measuring mitochondrial oxygen uptake utilizing Seahorse technology [25]. Using this plate-based respirometry platform, we measured basal respiratory activity of MIN6 cells, added glucose to monitor glucose-stimulated respiration, and inhibited the ATP synthase with oligomycin to estimate to what extent respiration is used to make ATP and how much of it is linked to mitochondrial proton leak. Fig. 2b depicts typical oxygen consumption traces, corrected for non-mitochondrial respiration, for the entire time course of the respiratory assay. Calculations for (non-) mitochondrial respiration, proton leak, ATP-linked respiration and coupling efficiency are described in Research Design and Methods. Low-glucose experiments (2 mM) that did not require additional glucose during the assay were run in separate wells from high-glucose (16.5 mM) experiments and were carefully time-matched. Mitochondrial

respiration at 2 and 16.5 mM glucose was not significantly different between *Drp1* KD and control cells (Fig. 2c), although glucose-stimulated respiration tended to be lower in *Drp1* KD cells (Fig. 2c). Interestingly, *Drp1* depletion from MIN6 cells lowered mitochondrial respiration that is used to make ATP at high glucose (Fig. 2d), a statistically significant effect reflected by decreased coupling efficiency of glucose-stimulated oxidative phosphorylation (Fig. 2e). This relatively low coupling efficiency also reflects an increase in mitochondrial proton leak that is provoked by *Drp1* KD at high glucose (Fig. 2f). Note that the concomitant changes in oxygen consumption linked to proton leak (increase) and ATP synthesis (decrease) neutralize each other, such that overall glucose-stimulated respiration does not differ significantly between *Drp1* KD and control cells (Fig. 2c). Since the bioenergetic effects of *Drp1* depletion are not caused by changes in respiratory chain components (suppl. Fig. 1a, b, c), impaired GSIS in the MIN6 cells upon *Drp1* KD is thus directly related to the decreased rate and coupling efficiency of glucose-stimulated oxidative phosphorylation. Consistently, *Drp1* KD decreases intracellular ATP content upon glucose stimulation by ~ 30% (Fig. 2g).

Pharmacological Drp1 inhibition corroborates the genetic *Drp1* KD phenotype

Long-term genetic inactivation of *Drp1* may well affect mitophagy and mitochondrial quality control, which confounds interpretation of *Drp1* KD effects on GSIS. Indeed, gene expression changes in the *Drp1* KD model suggest cellular adaptation (Fig. 1 f, k), which is why examined whether acute selective, chemical inhibition of *Drp1* that recapitulates the reduction of GSIS impairment caused by genetic *Drp1* silencing. The cell-permeant, small molecule mdivi-1 (mitochondrial division inhibitor-1) inhibits *Drp1* assembly and GTPase activity and has been previously suggested as a therapeutic for stroke, myocardial infarction and neurodegenerative diseases [26-29].

We preincubated MIN6 cells with 25 or 50 μM mdivi-1 at basal and stimulatory glucose levels and found that mdivi-1 has no effect on insulin content (Fig. 3a) or basal insulin release (Fig. 3b). GSIS, however, is dose-dependently lowered by mdivi-1, reaching statistical significance at 50 μM (Fig. 3b). These mdivi-1 effects echo those observed after *Drp1* KD (Fig. 2a). Equally, mdivi-1 fully mimicked the bioenergetic effects of *Drp1* KD: basal and glucose-stimulated respiration was unaffected by 50μM mdivi-1 (Fig. 3c), while mitochondrial proton leak was increased (Fig. 3d) and respiration used to make ATP was decreased (Fig. 3e). Consequently, mdivi-1 blunts the coupling efficiency of glucose-stimulated oxidative phosphorylation (Fig. 3f). Increasing the mdivi-1 dose to 100 μM had no further impact on the bioenergetics of the MIN6 cells, suggesting that 50 μM represents the fully inhibitory dose (suppl. Fig. 2). To investigate the translational potential of fission-dependent GSIS, we incubated human pancreatic islets with mdivi-1 and, consistent with the cellular data, observed no effect on insulin content or basal insulin release but saw a significant decrease of GSIS (Fig. 4a, b, c). These results collectively demonstrate that inhibition of *Drp1*-mediated mitochondrial fission by mdivi-1 controls GSIS in both human pancreatic islets and cultured β-cells.

Mdivi-1 decreases GSIS in pancreatic islets by decreasing oxidative capacity

To explore the physiological and pathological relevance of *Drp1*, we studied the effect of mdivi-1 treatment on islets isolated from mice. Consistent with human islet and MIN6 cell data, mdivi-1 did not alter insulin content but attenuated GSIS (Fig. 4d, e, f). Representative real-time respiratory measurements under control conditions in islet-capture plates are depicted in Fig. 4g (see Research Design and Methods). Mdivi-1 did not affect basal islet respiration at the low glucose concentration but significantly lowered glucose-stimulated respiration at the higher concentration (Fig.

4h). The lowered respiratory activity at high glucose was due to an mdivi-1-induced decrease of respiration linked to ATP synthesis (Fig. 4i), consistent with our results in MIN6 cells. Unlike its effect on cells, however, mdivi-1 left islet proton leak unaffected (Fig. 4j), which is why its inhibitory effect on ATP-synthesis-coupled respiration is apparent from the overall glucose-stimulated oxygen consumption in islets (Fig. 4h). Consequent to its lowering effect on glucose oxidation linked to ATP synthesis, mdivi-1 significantly decreased the coupling efficiency of mouse islets (Fig. 4k). Collectively, these data demonstrate that *Drp1* controls islet GSIS by regulating glucose oxidation, and not proton leak.

Pyruvate rescues impaired function of Drp1-deficient cells and islets

We hypothesized that the impaired glucose oxidation is likely secondary to reduced mitochondrial substrate supply, and we assessed this by directly providing pyruvate to mitochondria. We observed that the impaired GSIS of *Drp1*-depleted MIN6 cells could be entirely rescued by supplying the cells with exogenous pyruvate (Fig. 5a, b). This observation suggests that pyruvate either circumvents defects in glucose-fuelled ATP production or else triggers insulin secretion downstream of mitochondria. Pyruvate augments glucose-stimulated oxygen uptake in MIN6 cells irrespective of the presence of *Drp1* (Fig. 5c). The stimulatory effect of pyruvate on glucose oxidation was mirrored by a (not statistically significant) boost of GSIS in control and *Drp1*-depleted cells (Fig. 5a). Pyruvate stimulation restores ATP-synthesis-linked respiration in *Drp1*-deficient cells to the level seen in control cells incubated at high glucose (Fig. 5d). The restorative effect of pyruvate is not evident from coupling efficiency (Fig. 5e), which remained low after pyruvate supplementation because of the persistently high mitochondrial proton leak exhibited by *Drp1* KD cells (Fig. 5f). Pyruvate thus rescues GSIS despite relatively high proton leak activity, demonstrating

that GSIS impairment in *Drp1*-deficient cells is predominantly caused by decreased ATP synthesis ability. This conclusion is supported by the increased ATP content in pyruvate-treated cells (Fig. 5g, h). The restored ATP levels suggest that glucose-fueled oxidative phosphorylation in *Drp1*-deficient MIN6 cells is limited upstream of pyruvate; i.e., at the level of glycolysis. Glucose transporter gene expression and glucose uptake are not negatively affected in *Drp1* KD cells (Fig. 5i, j) and positive trends are rather suggesting deficiencies downstream of glucose transport. Interestingly, the use of glucokinase activator GKA50 improved glucose oxidation in *Drp1* KD cells and rescued GSIS (Fig. 5k, l).

It is difficult to gauge the translational potential of this pyruvate effect as native β-cells lack the monocarboxylate carrier protein that allows insulinoma cells to take up pyruvate [1]. Therefore, we tested the effect of pyruvate supplementation on mouse pancreatic islets treated with mdivi-1. GSIS deficiency was not rescued by sodium pyruvate in mouse pancreatic islets (Fig. 6a, b), thus excluding the possibility that pyruvate acts as an extracellular secretagogue that enhances secretory mechanisms downstream of mitochondria. However, GSIS impairment was entirely overcome by the membrane-permeant methyl pyruvate (Fig. 6a, b). Indeed, methyl pyruvate is also able to provoke insulin secretion in *Drp1*-inhibited mouse islets in the absence of glucose. One-hour incubation with methyl-pyruvate fully rescued the *Drp1*-dependent deficiency of triggered insulin secretion in the presence and absence of 16.5 mM glucose (Fig. 6a). The respective respiration measurements indicate that methyl-pyruvate acts as a mitochondrial substrate by increasing mitochondrial respiration (Fig. 6c). Despite some increase in proton leak respiration when glucose and methyl-pyruvate are combined (Fig. 6d), methyl pyruvate treatment overcomes Drp1-dependent differences in ATP-synthesis-linked respiration (Fig. 6e). Moreover, the

mdivi-1-invoked difference in coupling efficiency is ameliorated by methyl pyruvate treatment (Fig. 6f). These findings suggest a model (Fig. 6g) that predicts that direct substrate delivery to mitochondria may be pursued as a potential route for drug intervention to rescue fission-impaired GSIS.

Discussion

The present findings provide important insight into the mechanism by which the mitochondrial fission protein *Drp1* controls pancreatic insulin secretion. Specifically, the data demonstrate that *Drp1*-mediated mitochondrial fragmentation ensures that mitochondria are supplied with sufficient reducing power during GSIS. We demonstrate that *Drp1* deficiency does not directly impair glucose-stimulated oxidative phosphorylation, but instead limits mitochondrial ATP synthesis by compromising substrate delivery upstream of mitochondria. Unexpectedly, this limitation can be simply overcome by providing β-cells with exogenous pyruvate. This insight improves our basic understanding of the relationship between mitochondrial dynamics and function [30] as it demonstrates that mitochondrial morphology can influence bioenergetic processes (glycolysis) that operate outside and upstream from the organelle itself. The ability to rescue impaired mitochondrial ATP output by direct substrate delivery opens a new window for the development of compounds to treat mitochondrial disorders and, more specifically, defects in insulin secretion associated with mitochondrial dysfunction.

Consistent with previous observations in INS-1E rat insulinoma cells overexpressing dominant-negative *Drp1* [22], we found that *Drp1* deficiency, due either to genetic knockdown or pharmacological inhibition, lowers GSIS in MIN6 mouse insulinoma cells. This *Drp1*-deficiency phenotype was also exhibited by mouse and human pancreatic islets, thus highlighting the physiological and

translational relevance of *Drp1* control over GSIS. In agreement with the INS-1E cell data [22], we found that *Drp1* depletion from MIN6 cells increases mitochondrial respiration linked to proton leak and thus lowers coupling efficiency of oxidative phosphorylation. However, our plate-based respirometry analysis of adherent MIN6 cells disclosed that *Drp1* KD also causes a decrease of ATP-synthesis-coupled respiration, an effect that contributes to the relatively low coupling efficiency in *Drp1*-depleted cells. Our experiments thus demonstrate that *Drp1* impacts both glucose-fueled respiration used to make ATP and to drive proton leak. In a more physiologically relevant experimental model, the pancreatic mouse islet, we further found that *Drp1* inhibition resulted in marked reduction of ATP-synthesis-linked glucose oxidation without having an effect on proton leak. The islet data thus suggest that limited glucose-driven respiratory flux is the main explanation for impaired GSIS after *Drp1* inhibition rather than the increased proton leak that coincides with such limitation in cells. Indeed, our 'substrate rescue' experiments demonstrate that the GSIS defects exhibited by mitochondrial-fission-deficient MIN6 cells can be entirely overcome by pyruvate supplementation, despite the persistently elevated proton leak. Our data thus provide compelling evidence that glucose-stimulated oxidative phosphorylation in mitochondrial-fission-deficient beta cells is largely controlled by mitochondrial substrate delivery, as pyruvate supplementation rescues respiration, ATP output and insulin secretion, all of which were compromised after *Drp1* silencing. Similarly cell-permeant methyl-pyruvate rescues respiration, coupling efficiency and insulin secretion in mdivi-1 treated islets. Further work, possibly involving global metabolomics approaches, is required on the crucial rate-limiting steps of substrate supply. Our study excludes compromised glucose availability as glucose uptake was increased, not decreased, in *Drp1* KD cells. Interestingly,

glucokinase activator GKA50 rescued respiration and insulin secretion in MIN6 cells, an observation that supports the concept of lowered glucose catabolism but that requires experimental confirmation in pancreatic islets. Future studies should also consider compromised shuttling of glycolytic NADH to the mitochondrial matrix. Although the rescue by pyruvate argues against a role for the mitochondrial pyruvate carrier (MPC) during limited substrate supply in *Drp1*-deficient systems, restricted pyruvate transport can also not be formally excluded at this stage.

Our experiments highlight how modern technologies for measuring cellular and islet bioenergetics (such as real-time multi-well-plate-based respirometry) improve our understanding of insulin secretion by pancreatic β-cells. Nutrient-secretion coupling depends to a large degree on the link between glucose catabolism and ATP-triggered signaling events that lead to the exocytosis of insulin-containing granules. The strength of nutrient-secretion coupling is largely determined by the extent to which energy liberated during glucose combustion is used to make ATP, and by how much of it is wasted via mitochondrial proton leak. Coupling efficiency of oxidative phosphorylation is an often underestimated bioenergetic parameter that is highly critical for β-cell biology as it quantifies the proportion of glucose-fueled respiration that is coupled to ATP synthesis. As coupling efficiency is an internally normalized parameter, it benefits from a comparably high signal-to-noise ratio that renders it exquisitely sensitive to *any* perturbation in proton leak, mitochondrial ATP synthesis and/or cellular substrate oxidation [31]. Indeed, changes in coupling efficiency following *Drp1* silencing underpin our discovery that glycolytic substrate delivery to mitochondria is the single parameter that controls insulin secretion, while direct effects on energy transduction (proton leak) play a minor role.

Other players in the mitochondrial fission-fusion system, such as *Opa1* [32], also have profound effects on GSIS. Whether or not these effects can be neutralized by substrate supplementation or stimulation of fusion genes such as mitofusin (*Mfn*), or if pathological changes in mitochondrial dynamics may more generally be rescued by increased substrate delivery, are questions that should be considered for future studies. In this respect, it has recently been reported that cellular energy deficiency induces mitochondrial fission via *AMPK*-dependent *Fis1* and *Drp1* recruitment [33]. This fission has been interpreted as being prerequisite for the removal of faulty mitochondria by mitophagy [33], but our findings offer the alternative possibility that mitochondrial fragmentation enhances glycolytic metabolite delivery to mitochondria and thus maintains ATP output during times of high energetic demand. In conclusion, mitochondrial dynamics exert profound control over cellular bioenergetics, and while influencing mitochondrial activity *per se*, also affect upstream energetic processes such as substrate delivery.

Authors Contribution

U.K. and M.J. conceptualized the research plan and analyzed all results; U.K. conducted most cell culture and mouse experiments; K.P. conducted the perfusion of mouse for islet isolation; A.M. conducted the experiments with human islets; O.K. provided human islets; S.K. performed cell culture experiments, D.L. performed seahorse experiments and glucose uptake; M.G. advised microscopic experiments,; M.H.T. and H.K. contributed reagents/materials/analytic tools and gave advice on experimental design; U.K., M.J., S.K., S.C.W. and C.A. interpreted all experiments and wrote the manuscript. M.J. is the guarantor of this work and, as such, had full access to all the data in the study and takes responsibility for the integrity of the data and the accuracy of the data analysis.

Acknowledgments

We thank Mrs Ruchi Jain and Ms Maria Kutschke at the Helmholtz Zentrum for excellent technical assistance; this work was supported in part by funding to MJ from the German Diabetes Center (DZD), to MHT from the Alexander von Humboldt Foundation, the Helmholtz Alliance ICEMED – Imaging and Curing Environmental Metabolic Diseases, through the Initiative and Networking Fund of the Helmholtz Association, and the Helmholtz cross-program topic "Metabolic Dysfunction". We are thankful to the European Consortium for Islet Transplantation for providing human islets. H.L. and O.K. have received funding for the HumEn project from the European Union's Seventh Framework Programme for Research, Technological Development and Demonstration under grant agreement No. 602587 (http://www.hum-en.eu/). No potential conflicts of interest relevant to this article were reported.

Figure legends

Figure 1. (a, b) Knockdown of *Drp1* using lentiviral expression vectors. MIN6 cells were infected with non-target vector (black bars) or *Drp1* shRNA (white bars) lenti-virus and selected for stable cell lines. (a) Knockdown efficiency was confirmed by qPCR. Data are represented as mean ±SEM (n=3). (b) Immunoblot and quantification of *Drp1* protein content. Tubulin was used as a loading control (n=4). (c) Relative levels of *Mfn1*, *Mfn2* and *Opa1* mRNA were measured by RT-qPCR after knockdown of *Drp1* in MIN6 cells. *HPRT* was used as a control for each sample. Data are represented as mean ±SEM (n=3). (d, e) Live confocal imaging of stably infected MIN6 cells that were stained with Mito Tracker red FM for 30 min. Representative confocal images of the non-targeted vector (d) and *Drp1* KD cells (e). (f) Immunoblot

and densitometric quantification of protein from various oxidative phosphorylation subunits in *Drp1* KD vs. non-target vector MIN6 cells (n= 3). (g) Insulin content in *Drp*1 KD MIN6 cells measured with Insulin-ELISA. Data are represented as mean ±SEM (n=4). (h) Relative levels of *Ins1* and *Ins2* mRNA were measured by RT-qPCR after knockdown of *Drp1* in MIN6 cells. *HPRT* was used as a control for each sample. Data are represented as mean ±SEM (n=3) and n-values represent independent experiments. Statistical significance of mean differences was tested by unpaired 2-tailed student t-test. $P<0.05$ (*), $P<0.01$ (**), $P<0.001$ (***).

Figure 2. Glucose-stimulated insulin secretion and bioenergetics of MIN6 cells. MIN6 cells stably infected with non-target vector (black bars) and *Drp1* shRNA (white bars) lenti-virus were exposed to either 2 or 16.5 mM glucose. (a) Insulin release was measured after 2 h in the presence of different secretagogues. Data are represented as mean ±SEM (n=4). (b) Right panel: Averaged time-resolved oxygen consumption traces measured using the XF24 extracellular flux analyzer as described in the methods. Left panel: Schematic representation marking different oxygen consumption modules. (c) Mitochondrial respiration in response to 2 and 16.5 mM glucose. (d) ATP-linked respiration. (e) Coupling efficiency. (f) Proton leak respiration and (g) ATP content. Data are represented as mean ±SEM (n=6; n=4 for g) and n-values represent independent experiments. Statistical significance of mean differences was tested by unpaired 2-tailed student t-test. $P<0.05$ (*), $P<0.01$ (**), $P<0.001$ (***).

Figure 3. Mdivi-1 effects in MIN6 cell culture and human pancreatic islets. (a-f) MIN6 cells were exposed to either 2 or 16.5 mM glucose with /without mdivi-1. (a) Insulin content at different doses of mdivi-1. (b) Insulin release at different doses of mdivi-1. Data are represented as mean ±SEM (n=4). (c) Mitochondrial respiration. (d)

Proton leak respiration. (e) ATP-linked respiration and (f) Coupling efficiency. Data are represented as mean ±SEM (n=5) and n-values represent independent experiments. Statistical significance of mean differences was tested by unpaired 2-tailed student t-test to compare two variables, and one-way ANOVA (with Bonferroni posthoc analysis) was used for multiple comparisons. $P<0.05$ (*), $P<0.01$ (**), $P<0.001$ (***).

Figure 4. Mdivi-1 action on insulin secretion and mitochondrial bioenergetics in pancreatic islets. (a-c) Human pancreatic islets were incubated with 2 and 16.5 mM glucose with /without mdivi-1. (a) Insulin content, (b) insulin secretion, and (c) insulin secretion normalized to insulin content are depicted. (d-k) Mouse pancreatic islets: (d-f) Batches of 8 size-matched islets were exposed to either 2 or 16.5 mM glucose with/without mdivi-1. After incubation, supernatant and lysates were collected for (d) insulin content, (e) insulin secretion, and (f) insulin secretion normalized to insulin content. Data are represented as means ±SEM of three independent experiments (n=3). (g) Representative scheme of time-resolved oxygen consumption traces of mouse wildtype pancreatic islets using islet-capture plates of the XF24 extracellular flux analyzer. (h) Mitochondrial respiration at low (2 mM) and high (16.5 mM) glucose. (i) ATP-linked respiration. (j) Proton leak respiration and (k) Coupling efficiency. Data are represented as means ±SEM (n=5) and n-values represent independent experiments. Statistical significance of mean differences was tested by unpaired 2-tailed student t-test. $P<0.05$ (*), $P<0.01$ (**), $P<0.001$ (***).

Figure 5. Pyruvate rescues *Drp1*-related deficiency in insulin secretion and bioenergetics in MIN6 cells. (a-k) MIN6 cells with non-target vector (black bars) and *Drp1* shRNA (white bars) lenti-virus were exposed to glucose (2 and 16.5 mM) or sodium-pyruvate (10 mM) for 2 h. (a) Insulin secretion. (b) Insulin secretion

expressed as percentage of non-target vector (control). (c) Mitochondrial respiration. (d) ATP-linked respiration. (e) Coupling efficiency. (f) Proton leak respiration. (g) Intracelllular ATP content. (h) Intracellular ATP content expressed as percentage of non-target vector (control). (i) Relative levels of *Glut1*, *Glut2* and *Gck* mRNA were measured by RT-qPCR in wildtype and *Drp1* KD MIN6 cells. *HPRT* was used as housekeeping gene. (j) Glucose uptake of MIN6 cells. (k-l) Effect of glucokinase activator GKA 50 on (k) insulin secretion and (l) oxygen consumption rates. Data are represented as means ±SEM (n=4) and n-values represent independent experiments. Statistical significance of mean differences was tested by unpaired 2-tailed student t- to compare two variables, and one-way ANOVA (with Bonferroni posthoc analysis) was used for multiple comparisons. $P<0.05$ (*), $P<0.01$ (**), $P<0.001$ (***).

Figure 6. Methyl-pyruvate rescues *Drp1*-related deficiency in insulin secretion and bioenergetics in pancreatic mouse islets. (a, b) Batches of eight size-matched islets were exposed to different substrates/secretagogues with /without mdivi-1. After incubation, supernatant was collected to measure (a) Insulin secretion and (b) Insulin secretion normalized to basal control. Data are represented as means ±SEM (n=3). (c) Mitochondrial respiration. (d) Proton leak respiration. (e) ATP-linked respiration and (f) Coupling efficiency (g) Schematic model of the impact of *Drp1* during GSIS, emphazising the rescue of insulin secretion with pyruvate. Statistical significance of mean differences was tested by unpaired 2-tailed student t- to compare two variables, and one-way ANOVA (with Bonferroni posthoc analysis) was used for multiple comparisons. $P<0.05$ (*), $P<0.01$ (**), $P<0.001$ (***).

References

1. Rutter GA, Pullen TJ, Hodson DJ, Martinez-Sanchez A: **Pancreatic beta-cell identity, glucose sensing and the control of insulin secretion**. *Biochem J* 2015, **466**(2):203-218.
2. Ashcroft FM, Proks P, Smith PA, Ammala C, Bokvist K, Rorsman P: **Stimulus-secretion coupling in pancreatic beta cells**. *J Cell Biochem* 1994, **55 Suppl**:54-65.
3. Maechler P, Li N, Casimir M, Vetterli L, Frigerio F, Brun T: **Role of mitochondria in beta-cell function and dysfunction**. *Adv Exp Med Biol* 2010, **654**:193-216.
4. Molina AJ, Wikstrom JD, Stiles L, Las G, Mohamed H, Elorza A, Walzer G, Twig G, Katz S, Corkey BE *et al*: **Mitochondrial networking protects beta-cells from nutrient-induced apoptosis**. *Diabetes* 2009, **58**(10):2303-2315.
5. Chan DC: **Mitochondria: dynamic organelles in disease, aging, and development**. *Cell* 2006, **125**(7):1241-1252.
6. Hoppins S, Lackner L, Nunnari J: **The machines that divide and fuse mitochondria**. *Annu Rev Biochem* 2007, **76**:751-780.
7. Chan DC: **Fusion and fission: interlinked processes critical for mitochondrial health**. *Annu Rev Genet* 2012, **46**:265-287.
8. Chen H, Chan DC: **Emerging functions of mammalian mitochondrial fusion and fission**. *Hum Mol Genet* 2005, **14 Spec No. 2**:R283-289.
9. Mishra P, Chan DC: **Metabolic regulation of mitochondrial dynamics**. *J Cell Biol* 2016.
10. Alexander C, Votruba M, Pesch UE, Thiselton DL, Mayer S, Moore A, Rodriguez M, Kellner U, Leo-Kottler B, Auburger G *et al*: **OPA1, encoding a dynamin-related GTPase, is mutated in autosomal dominant optic atrophy linked to chromosome 3q28**. *Nat Genet* 2000, **26**(2):211-215.
11. Waterham HR, Koster J, van Roermund CW, Mooyer PA, Wanders RJ, Leonard JV: **A lethal defect of mitochondrial and peroxisomal fission**. *N Engl J Med* 2007, **356**(17):1736-1741.
12. Zuchner S, Mersiyanova IV, Muglia M, Bissar-Tadmouri N, Rochelle J, Dadali EL, Zappia M, Nelis E, Patitucci A, Senderek J *et al*: **Mutations in the mitochondrial GTPase mitofusin 2 cause Charcot-Marie-Tooth neuropathy type 2A**. *Nat Genet* 2004, **36**(5):449-451.
13. Anello M, Lupi R, Spampinato D, Piro S, Masini M, Boggi U, Del Prato S, Rabuazzo AM, Purrello F, Marchetti P: **Functional and morphological alterations of mitochondria in pancreatic beta cells from type 2 diabetic patients**. *Diabetologia* 2005, **48**(2):282-289.
14. Smirnova E, Griparic L, Shurland DL, van der Bliek AM: **Dynamin-related protein Drp1 is required for mitochondrial division in mammalian cells**. *Mol Biol Cell* 2001, **12**(8):2245-2256.
15. Lackner LL, Nunnari JM: **The molecular mechanism and cellular functions of mitochondrial division**. *Biochim Biophys Acta* 2009, **1792**(12):1138-1144.
16. Chang CR, Blackstone C: **Drp1 phosphorylation and mitochondrial regulation**. *EMBO Rep* 2007, **8**(12):1088-1089; author reply 1089-1090.
17. Santel A, Frank S: **Shaping mitochondria: The complex posttranslational regulation of the mitochondrial fission protein DRP1**. *IUBMB Life* 2008, **60**(7):448-455.

18. Liu J, Chen Z, Zhang Y, Zhang M, Zhu X, Fan Y, Shi S, Zen K, Liu Z: **Rhein protects pancreatic beta-cells from dynamin-related protein-1-mediated mitochondrial fission and cell apoptosis under hyperglycemia**. *Diabetes* 2013, **62**(11):3927-3935.
19. Men X, Wang H, Li M, Cai H, Xu S, Zhang W, Xu Y, Ye L, Yang W, Wollheim CB *et al*: **Dynamin-related protein 1 mediates high glucose induced pancreatic beta cell apoptosis**. *Int J Biochem Cell Biol* 2009, **41**(4):879-890.
20. Peng L, Men X, Zhang W, Wang H, Xu S, Fang Q, Liu H, Yang W, Lou J: **Involvement of dynamin-related protein 1 in free fatty acid-induced INS-1-derived cell apoptosis**. *PLoS One* 2012, **7**(11):e49258.
21. Peng L, Men X, Zhang W, Wang H, Xu S, Xu M, Xu Y, Yang W, Lou J: **Dynamin-related protein 1 is implicated in endoplasmic reticulum stress-induced pancreatic beta-cell apoptosis**. *Int J Mol Med* 2011, **28**(2):161-169.
22. Jhun BS, Lee H, Jin ZG, Yoon Y: **Glucose stimulation induces dynamic change of mitochondrial morphology to promote insulin secretion in the insulinoma cell line INS-1E**. *PLoS One* 2013, **8**(4):e60810.
23. Carter JD, Dula SB, Corbin KL, Wu R, Nunemaker CS: **A practical guide to rodent islet isolation and assessment**. *Biol Proced Online* 2009, **11**:3-31.
24. Divakaruni AS, Paradyse A, Ferrick DA, Murphy AN, Jastroch M: **Analysis and interpretation of microplate-based oxygen consumption and pH data**. *Methods Enzymol* 2014, **547**:309-354.
25. Affourtit C, Brand MD: **Measuring mitochondrial bioenergetics in INS-1E insulinoma cells**. *Methods Enzymol* 2009, **457**:405-424.
26. Lackner LL, Nunnari J: **Small molecule inhibitors of mitochondrial division: tools that translate basic biological research into medicine**. *Chem Biol* 2010, **17**(6):578-583.
27. Manczak M, Reddy PH: **Mitochondrial division inhibitor 1 protects against mutant huntingtin-induced abnormal mitochondrial dynamics and neuronal damage in Huntington's disease**. *Hum Mol Genet* 2015, **24**(25):7308-7325.
28. Zaja I, Bai X, Liu Y, Kikuchi C, Dosenovic S, Yan Y, Canfield SG, Bosnjak ZJ: **Cdk1, PKCdelta and calcineurin-mediated Drp1 pathway contributes to mitochondrial fission-induced cardiomyocyte death**. *Biochem Biophys Res Commun* 2014, **453**(4):710-721.
29. Zhao YX, Cui M, Chen SF, Dong Q, Liu XY: **Amelioration of ischemic mitochondrial injury and Bax-dependent outer membrane permeabilization by Mdivi-1**. *CNS Neurosci Ther* 2014, **20**(6):528-538.
30. Liesa M, Shirihai OS: **Mitochondrial dynamics in the regulation of nutrient utilization and energy expenditure**. *Cell Metab* 2013, **17**(4):491-506.
31. Brand MD, Nicholls DG: **Assessing mitochondrial dysfunction in cells**. *Biochem J* 2011, **435**(2):297-312.
32. Zhang Z, Wakabayashi N, Wakabayashi J, Tamura Y, Song WJ, Sereda S, Clerc P, Polster BM, Aja SM, Pletnikov MV *et al*: **The dynamin-related GTPase Opa1 is required for glucose-stimulated ATP production in pancreatic beta cells**. *Mol Biol Cell* 2011, **22**(13):2235-2245.
33. Toyama EQ, Herzig S, Courchet J, Lewis TL, Jr., Loson OC, Hellberg K, Young NP, Chen H, Polleux F, Chan DC *et al*: **Metabolism. AMP-activated**

protein kinase mediates mitochondrial fission in response to energy stress. *Science* 2016, **351**(6270):275-281.

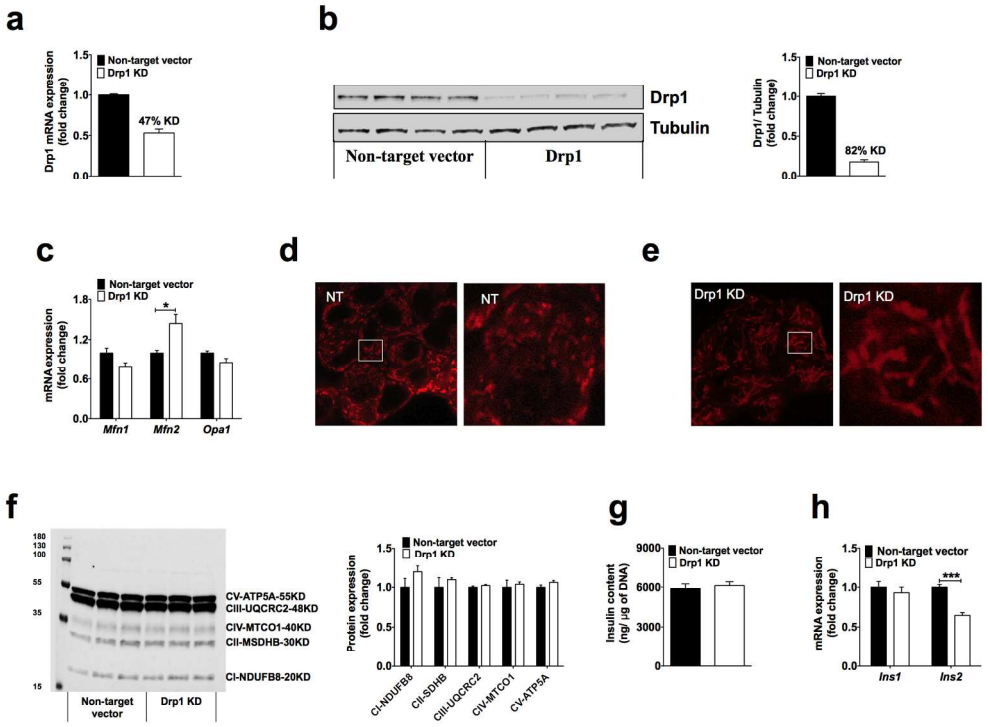

Figure 1. (a, b) Knockdown of Drp1 using lentiviral expression vectors. MIN6 cells were infected with non-target vector (black bars) or Drp1 shRNA (white bars) lenti-virus and selected for stable cell lines. (a) Knockdown efficiency was confirmed by qPCR. Data are represented as mean ±SEM (n=3). (b) Immunoblot and quantification of Drp1 protein content. Tubulin was used as a loading control (n=4). (c) Relative levels of Mfn1, Mfn2 and Opa1 mRNA were measured by RT-qPCR after knockdown of Drp1 in MIN6 cells. HPRT was used as a control for each sample. Data are represented as mean ±SEM (n=3). (d, e) Live confocal imaging of stably infected MIN6 cells that were stained with Mito Tracker red FM for 30 min. Representative confocal images of the non-targeted vector (d) and Drp1 KD cells (e). (f) Immunoblot and densitometric quantification of protein from various oxidative phosphorylation subunits in Drp1 KD vs. non-target vector MIN6 cells (n= 3). (g) Insulin content in Drp1 KD MIN6 cells measured with Insulin-ELISA. Data are represented as mean ±SEM (n=4). (h) Relative levels of Ins1 and Ins2 mRNA were measured by RT-qPCR after knockdown of Drp1 in MIN6 cells. HPRT was used as a control for each sample. Data are represented as mean ±SEM (n=3) and n-values represent independent experiments. Statistical significance of mean differences was tested by unpaired 2-tailed student t-test. P<0.05 (*), P<0.01 (**), P<0.001 (***).

190x143mm (300 x 300 DPI)

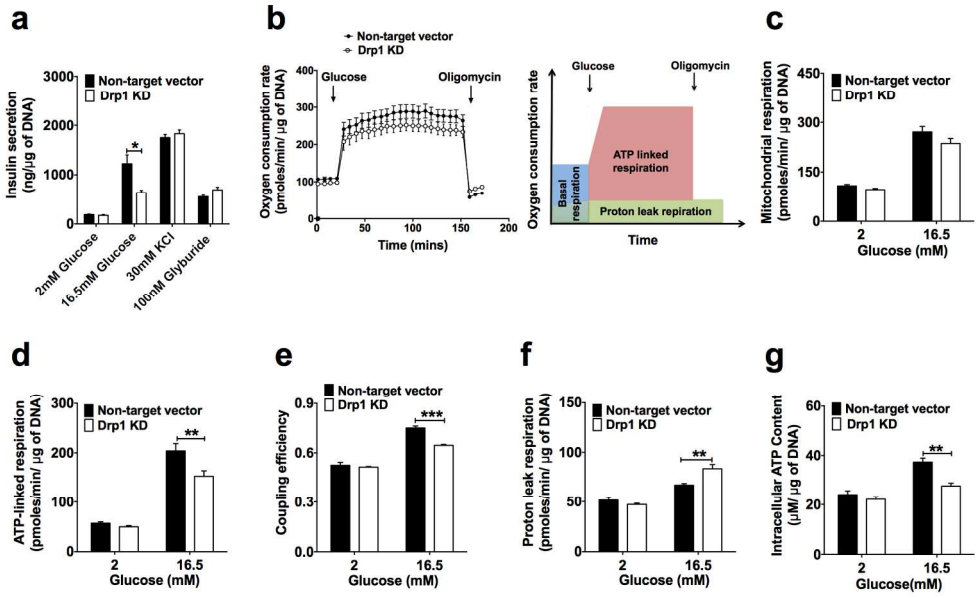

Figure 2. Glucose-stimulated insulin secretion and bioenergetics of MIN6 cells. MIN6 cells stably infected with non-target vector (black bars) and Drp1 shRNA (white bars) lenti-virus were exposed to either 2 or 16.5 mM glucose. (a) Insulin release was measured after 2 h in the presence of different secretagogues. Data are represented as mean ±SEM (n=4). (b) Right panel: Averaged time-resolved oxygen consumption traces measured using the XF24 extracellular flux analyzer as described in the methods. Left panel: Schematic representation marking different oxygen consumption modules. (c) Mitochondrial respiration in response to 2 and 16.5 mM glucose. (d) ATP-linked respiration. (e) Coupling efficiency. (f) Proton leak respiration and (g) ATP content. Data are represented as mean ±SEM (n=6; n=4 for g) and n-values represent independent experiments. Statistical significance of mean differences was tested by unpaired 2-tailed student t-test. P<0.05 (*), P<0.01 (**), P<0.001 (***).

193x117mm (300 x 300 DPI)

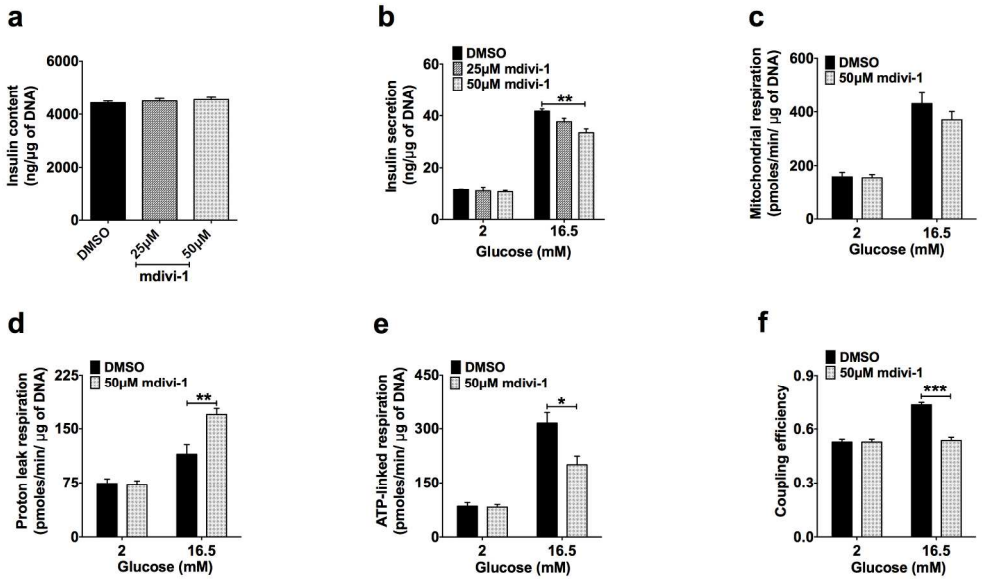

Figure 3. Mdivi-1 effects in MIN6 cell culture and human pancreatic islets. (a-f) MIN6 cells were exposed to either 2 or 16.5 mM glucose with /without mdivi-1. (a) Insulin content at different doses of mdivi-1. (b) Insulin release at different doses of mdivi-1. Data are represented as mean ±SEM (n=4). (c) Mitochondrial respiration. (d) Proton leak respiration. (e) ATP-linked respiration and (f) Coupling efficiency. Data are represented as mean ±SEM (n=5) and n-values represent independent experiments. Statistical significance of mean differences was tested by unpaired 2-tailed student t-test to compare two variables, and one-way ANOVA (with Bonferroni posthoc analysis) was used for multiple comparisons. $P<0.05$ (*), $P<0.01$ (**), $P<0.001$ (***).

219x129mm (300 x 300 DPI)

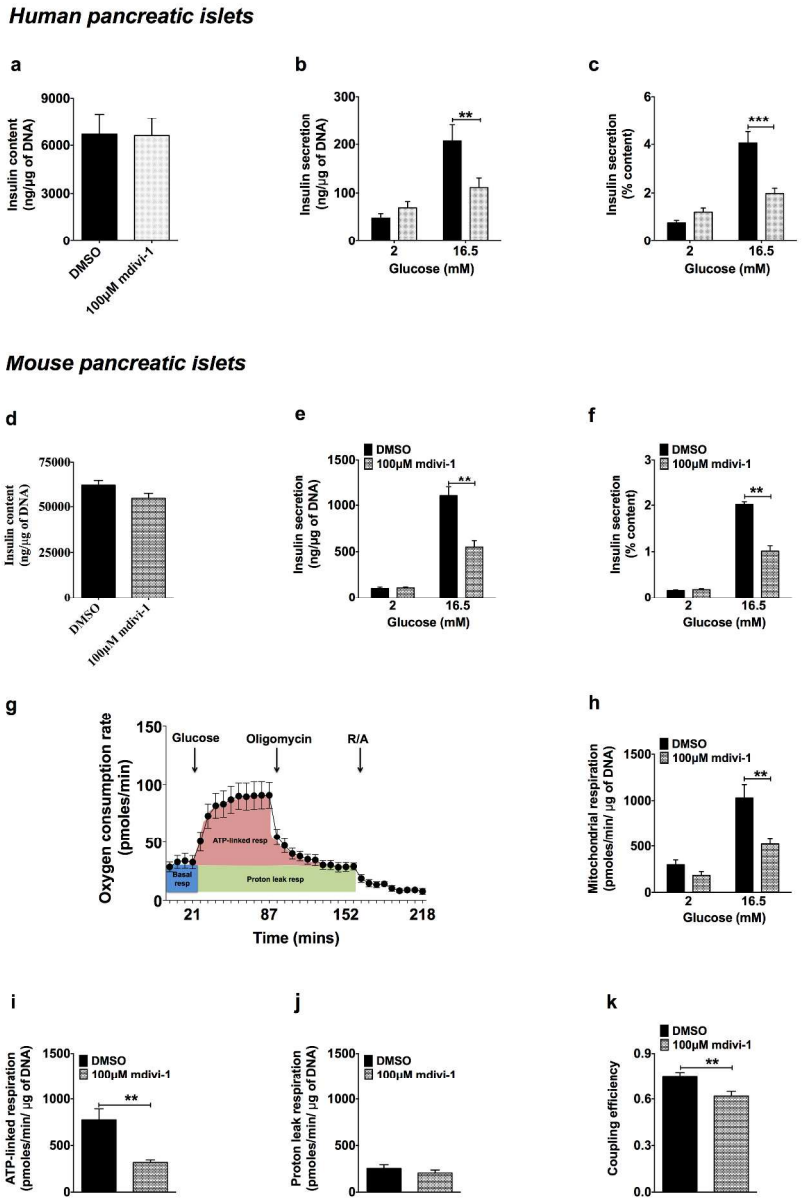

Figure 4. Mdivi-1 action on insulin secretion and mitochondrial bioenergetics in pancreatic islets. (a-c) Human pancreatic islets were incubated with 2 and 16.5 mM glucose with /without mdivi-1. (a) Insulin content, (b) insulin secretion, and (c) insulin secretion normalized to insulin content are depicted. (d-k) Mouse pancreatic islets: (d-f) Batches of 8 size-matched islets were exposed to either 2 or 16.5 mM glucose with/without mdivi-1. After incubation, supernatant and lysates were collected for (d) insulin content, (e) insulin secretion, and (f) insulin secretion normalized to insulin content. Data are represented as means ±SEM of three independent experiments (n=3). (g) Representative scheme of time-resolved oxygen consumption traces of mouse wildtype pancreatic islets using islet-capture plates of the XF24 extracellular flux analyzer. (h) Mitochondrial respiration at low (2 mM) and high (16.5 mM) glucose. (i) ATP-linked respiration. (j) Proton leak respiration and (k) Coupling efficiency. Data are represented as means ±SEM (n=5) and n-values represent independent experiments. Statistical significance of mean differences was tested by unpaired 2-tailed student t-test. P<0.05 (*), P<0.01 (**), P<0.001 (***).

267x390mm (300 x 300 DPI)

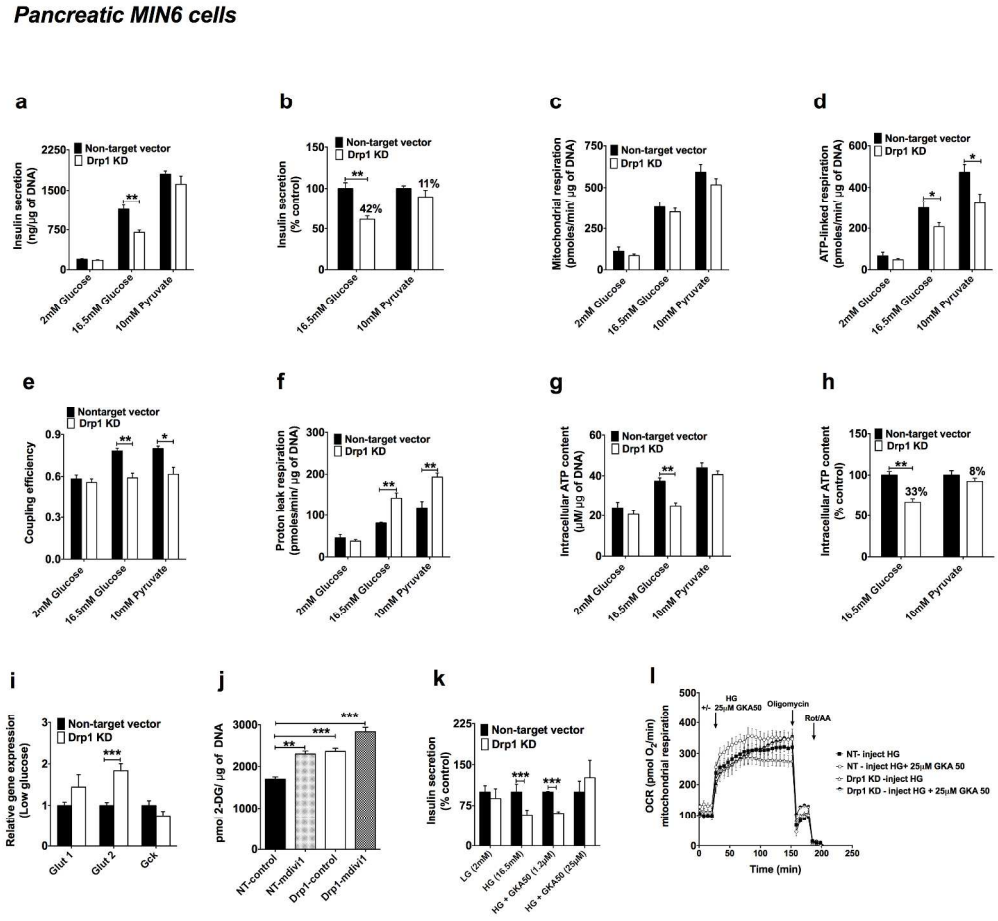

Figure 5. Pyruvate rescues Drp1-related deficiency in insulin secretion and bioenergetics in MIN6 cells. (a-k) MIN6 cells with non-target vector (black bars) and Drp1 shRNA (white bars) lenti-virus were exposed to glucose (2 and 16.5 mM) or sodium-pyruvate (10 mM) for 2 h. (a) Insulin secretion. (b) Insulin secretion expressed as percentage of non-target vector (control). (c) Mitochondrial respiration. (d) ATP-linked respiration. (e) Coupling efficiency. (f) Proton leak respiration. (g) Intracelllular ATP content. (h) Intracellular ATP content expressed as percentage of non-target vector (control). (i) Relative levels of Glut1, Glut2 and Gck mRNA were measured by RT-qPCR in wildtype and Drp1 KD MIN6 cells. HPRT was used as housekeeping gene. (j) Glucose uptake of MIN6 cells. (k-l) Effect of glucokinase activator GKA 50 on (k) insulin secretion and (l) oxygen consumption rates. Data are represented as means ±SEM (n=4) and n-values represent independent experiments. Statistical significance of mean differences was tested by unpaired 2-tailed student t- to compare two variables, and one-way ANOVA (with Bonferroni posthoc analysis) was used for multiple comparisons. P<0.05 (*), P<0.01 (**), P<0.001 (***).

285x264mm (300 x 300 DPI)

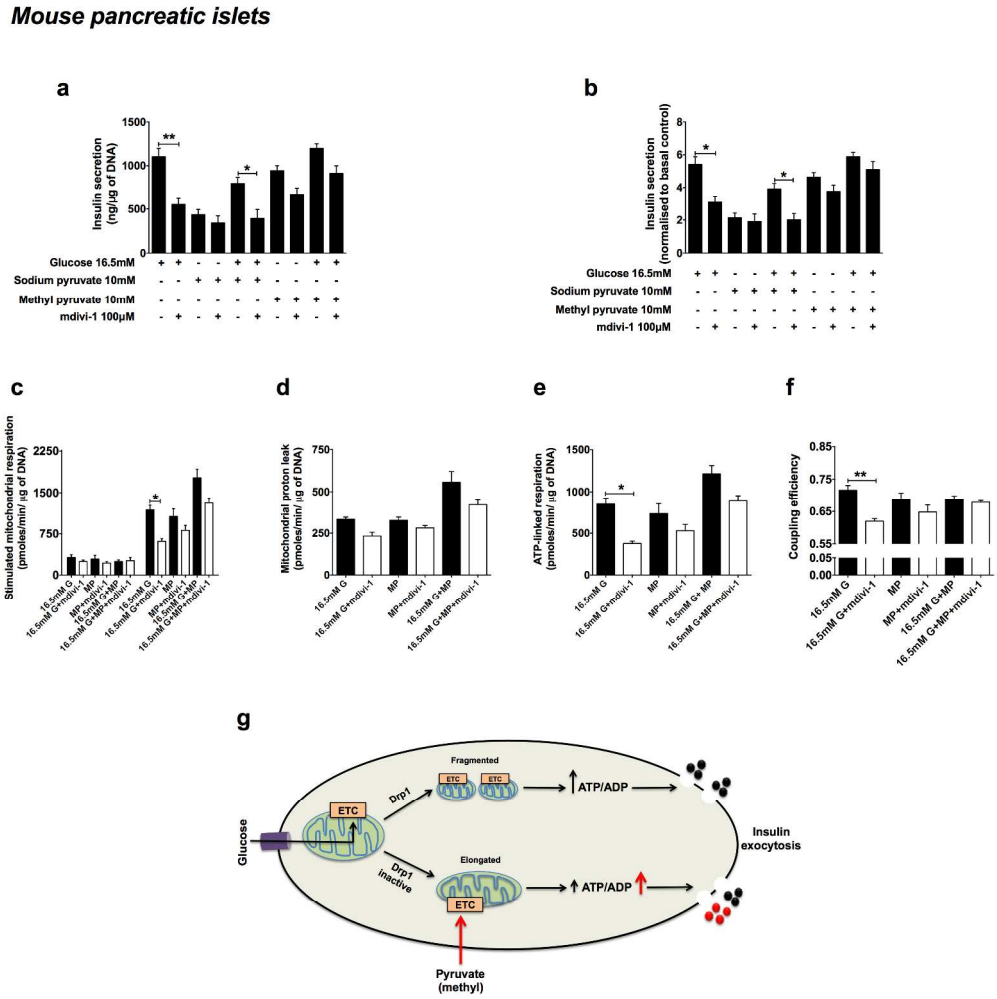

Figure 6. Methyl-pyruvate rescues Drp1-related deficiency in insulin secretion and bioenergetics in pancreatic mouse islets. (a, b) Batches of eight size-matched islets were exposed to different substrates/secretagogues with /without mdivi-1. After incubation, supernatant was collected to measure (a) Insulin secretion and (b) Insulin secretion normalized to basal control. Data are represented as means ±SEM (n=3). (c) Mitochondrial respiration. (d) Proton leak respiration. (e) ATP-linked respiration and (f) Coupling efficiency (g) Schematic model of the impact of Drp1 during GSIS, emphasising the rescue of insulin secretion with pyruvate. Statistical significance of mean differences was tested by unpaired 2-tailed student t- to compare two variables, and one-way ANOVA (with Bonferroni posthoc analysis) was used for multiple comparisons. P<0.05 (*), P<0.01 (**), P<0.001 (***).

270x271mm (300 x 300 DPI)

Online supplemental data

Direct substrate delivery into mitochondrial-fission deficient pancreatic islets rescues insulin secretion

Uma D. Kabra[1,4], Katrin Pfuhlmann[1,4], Adriana Migliorini[1], Susanne Keipert[1], Daniel Lamp[1,4], Olle Korsgren[2], Moritz Gegg[1,4], Stephen C. Woods[5], Paul T. Pfluger[1], Heiko Lickert[1,4], Charles Affourtit[3], Matthias H. Tschöp[1,4], Martin Jastroch[1 *]

1. Supplementary figures

2. Supplementary experimental procedures

e. Western blot analysis, RNA isolation and RT-PCR

f. Primer sequences

1. Supplementary figures

Supplementary figure 1

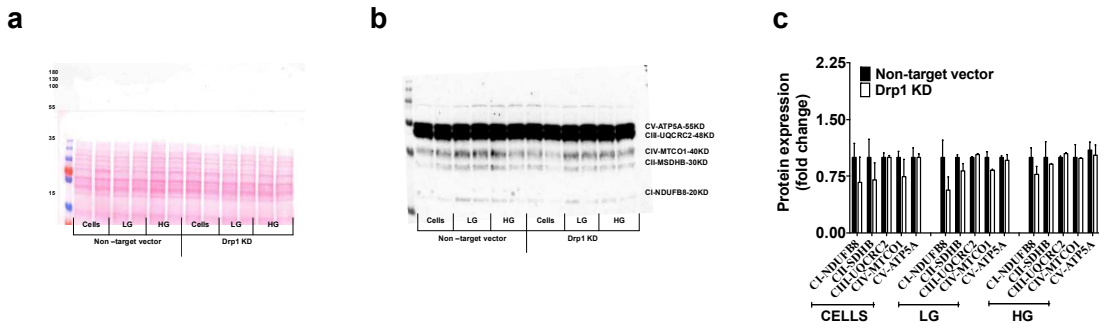

Supplementary figure 1. MIN6 cells stably infected with non-target vector (black bars) and *Drp1* shRNA (white bars) lenti-virus were exposed to 2 and 16.5 mM glucose for 2 h and probed for various subunits of the oxidative phosphorylation machinery (OXPHOS). (a) Ponceau staining of the Western membrane. (b) Immunoblot of OXPHOS protein detection. A representative Western blotting result is depicted. (c) Quantification of expression of OXPHOS proteins. Cell lysates (40 µg of protein per lane) were subjected to SDS-PAGE and blotted as described in methods (n= 3). Statistical significance of mean differences was tested by unpaired 2-tailed student t-test. $P<0.05$ (*), $P<0.01$ (**), $P<0.001$ (***).

Supplementary figure 2

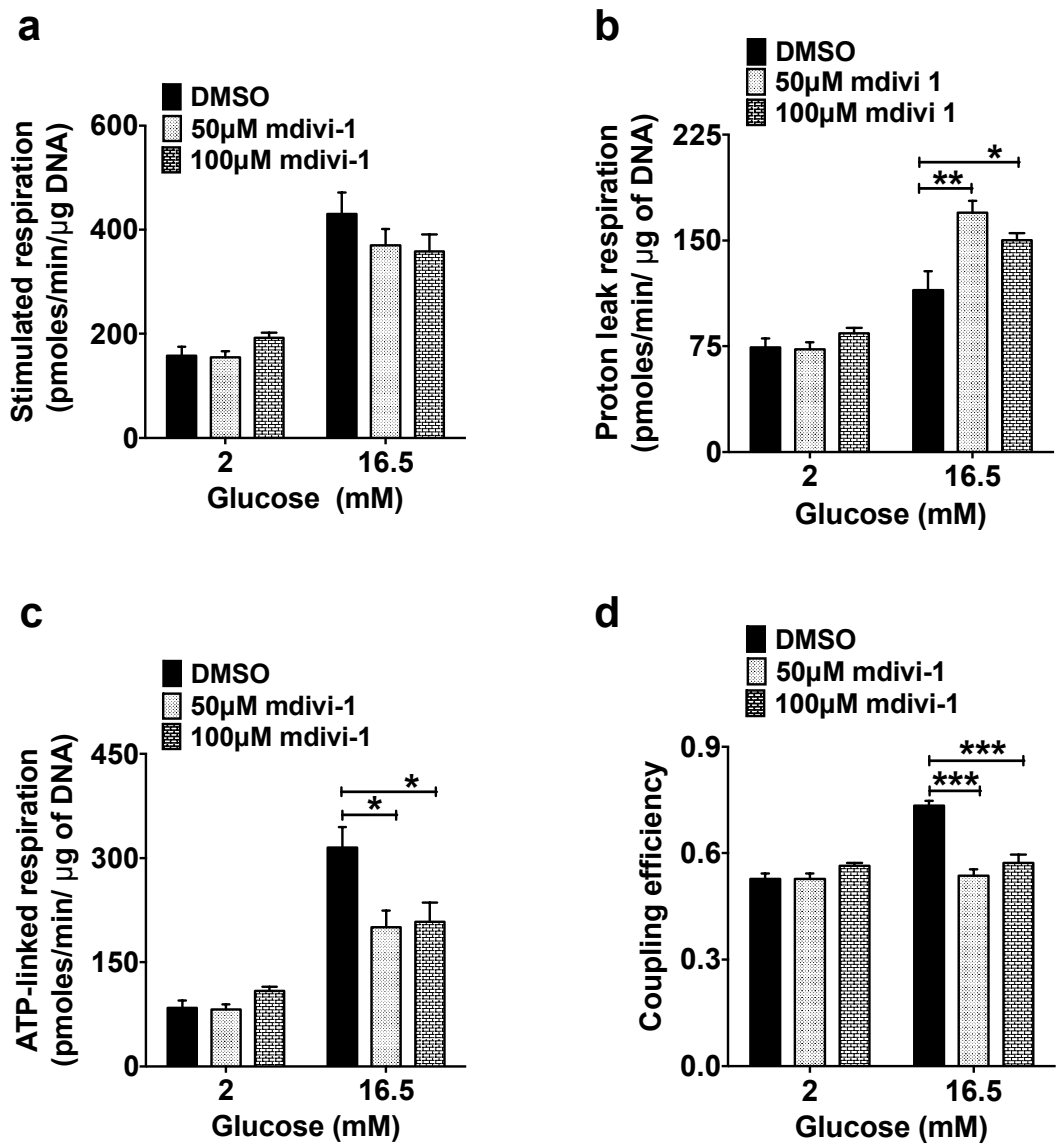

Supplementary figure 2. MIN6 cells were exposed to 2 and 16.5 mM glucose with /without mdivi-1 at 50 and 100 μM (a) Mitochondrial respiration (b) Proton leak respiration (c) ATP-linked respiration and (d) Coupling efficiency. Statistical significance of mean differences was tested by One-way ANOVA (Bonferroni) for multiple comparisons. $P<0.05$ (*), $P<0.01$ (**), $P<0.001$ (***).

Supplementary figure 3

a

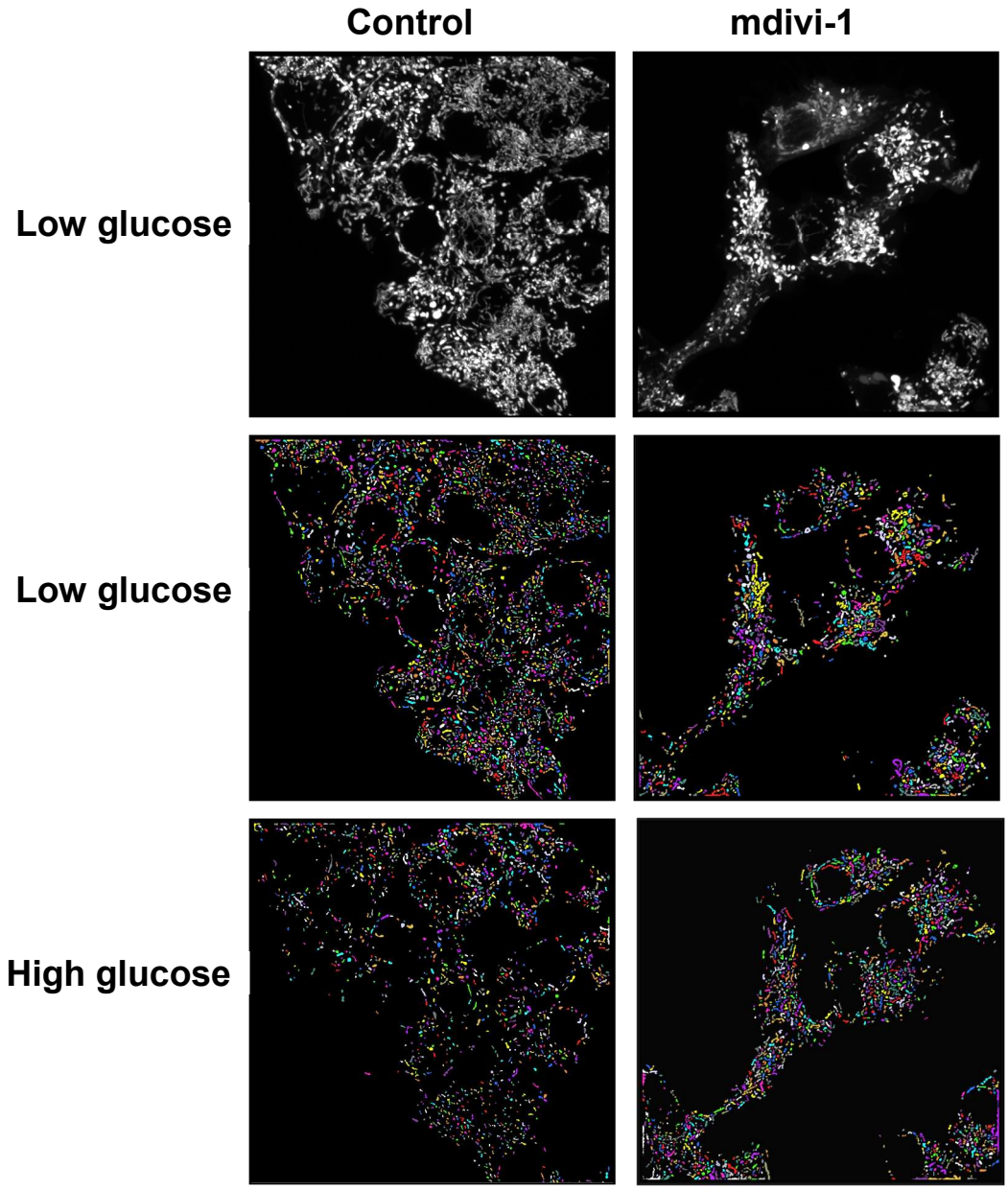

b

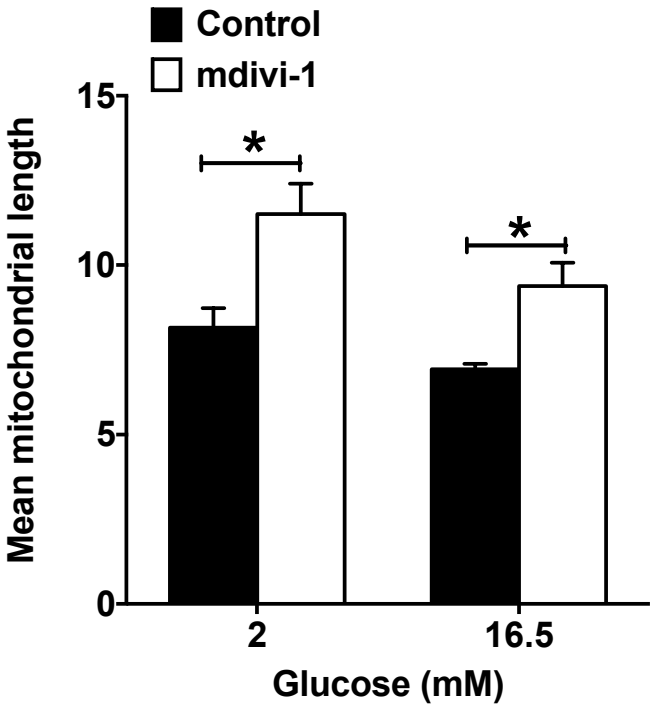

Supplementary figure 3. Effect of glucose on mitochondrial fragmentation in cultured MIN6 cells (a) MIN6 were plated 24 h prior experiment in i-treated ibidi chambers (8- well) at density of 70,000 cells/well in DMEM (1g/l glucose), 5% FBS and 1% P/S. Cells were then incubated with low glucose (2 mM) and high glucose (16.5 mM) with /without mdivi-1 and loaded with MitoTracker Red CMXRos (75 nM). The cells were washed with PBS and imaged with a Zeiss LSM880 Airyscan 63x objective. The images were processed using image analyst MKII (www.imageanalyst.net) to filter and binarize the images (2nd/3rd row images). (b) Mean mitochondrial length. The morphological pipeline "mean mitochondrial shape parameters" was applied to assess mean mitochondrial length of processed images. Average mean mitochondrial length is depicted in the bar charts and consists of three viewfields. Values are given as mean ± SEM (n = 3). Statistical significance of mean differences was tested by unpaired 2-tailed student t-test. P<0.05 (*), P<0.01 (**), P<0.001 (***).

Supplementary figure 4

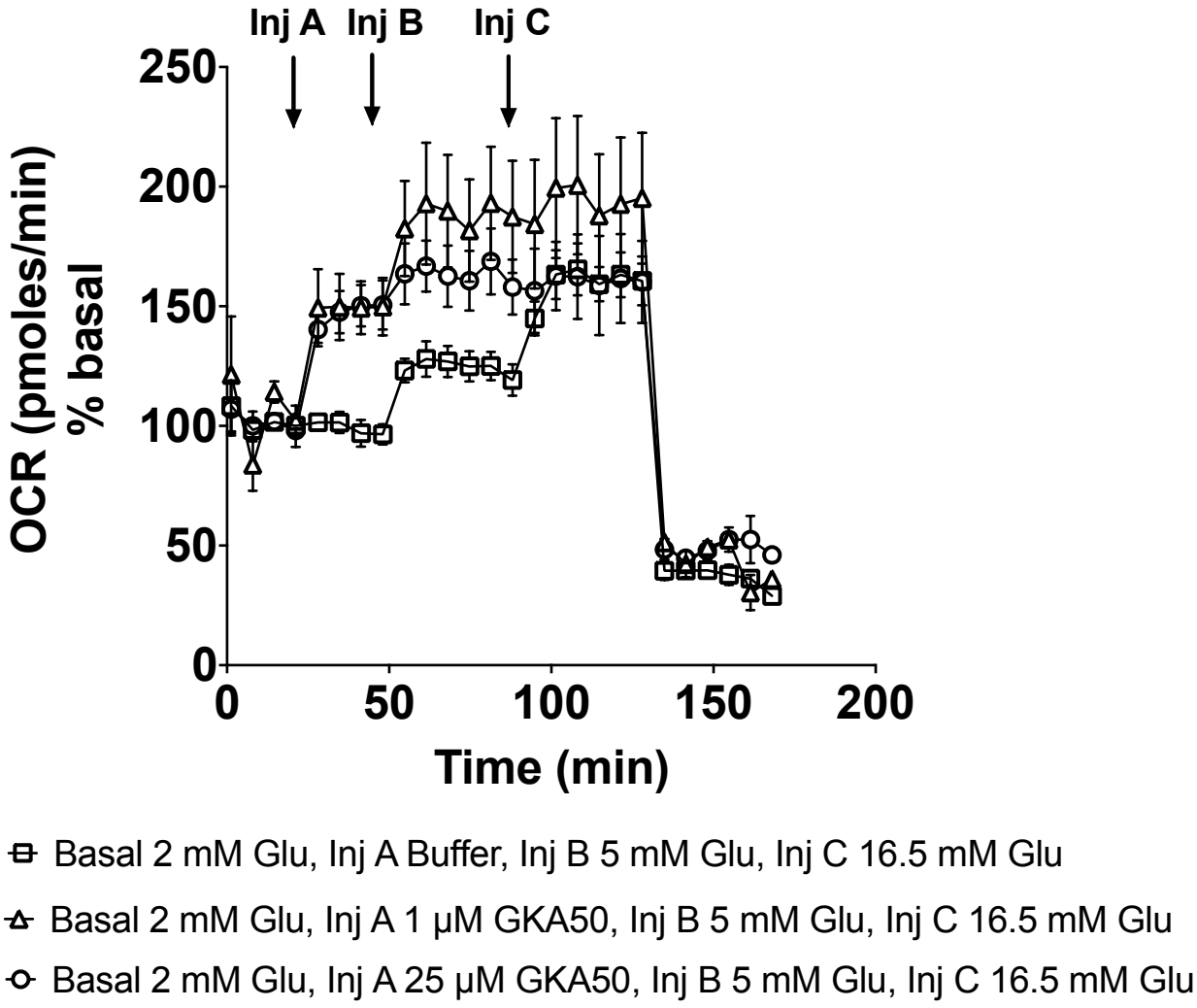

Supplementary figure 4. GKA50 increases glucose oxidation rates of MIN6 cells. Basal OCR rates of MIN6 cells were assessed at 2 mM glucose. Vehicle control, 1 or 25 µM Glucokinase activator GKA50 were injected in port A, followed by glucose injection in port B (adjusting glucose to 5 mM). Finally, glucose levels were adjusted to 16.5 mM by injection from port C. In port D, rotenone/antimycin A injection served to control for non-mitochondrial respiration.

Supplementary figure 5

a

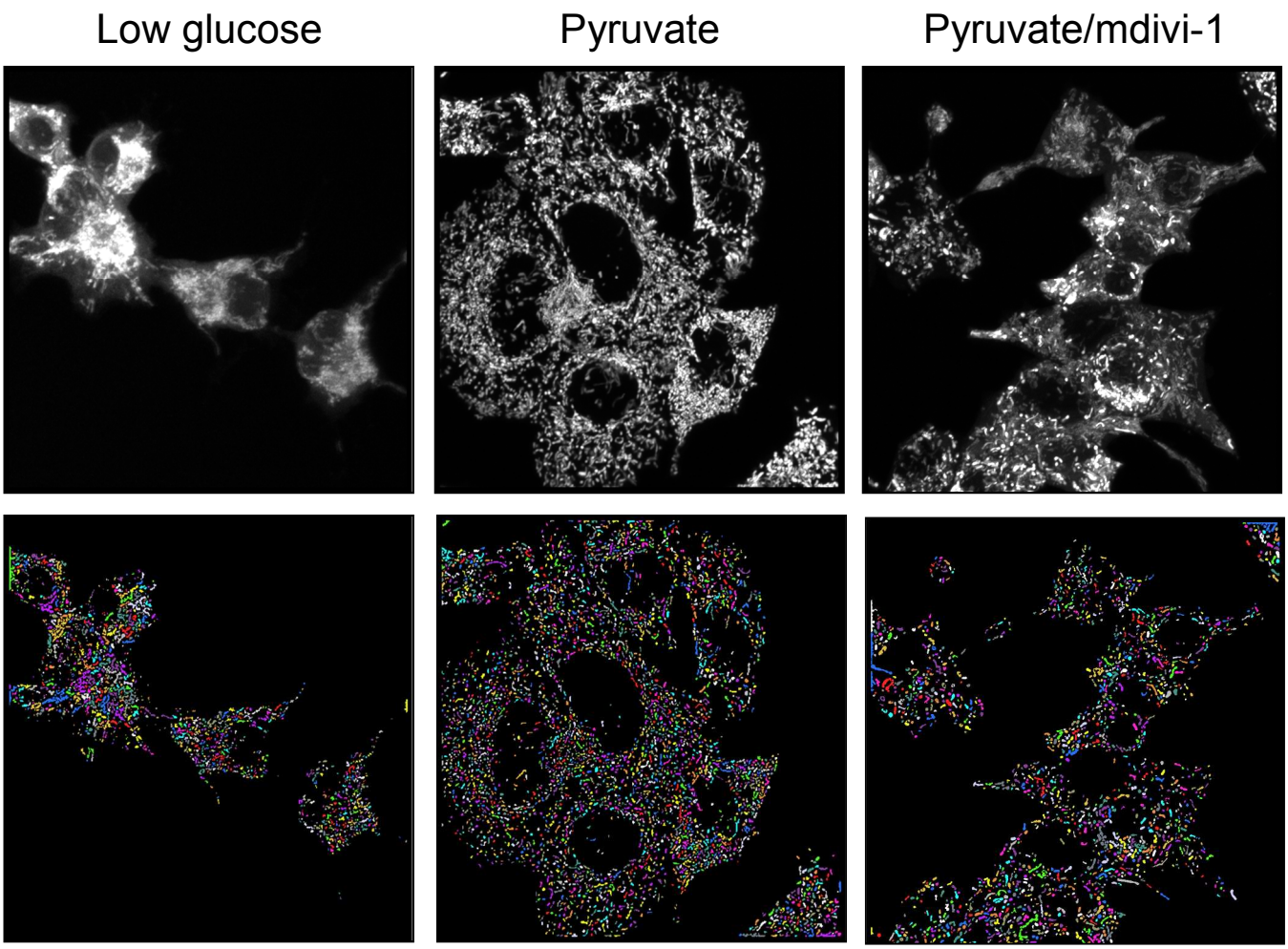

b

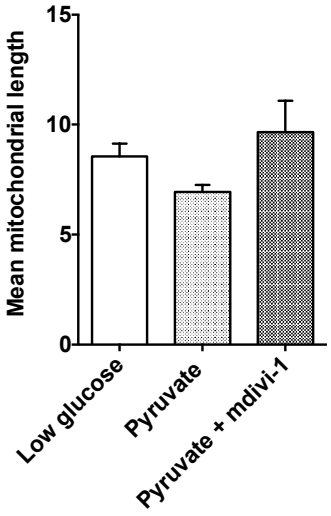

Supplementary figure 5. Effect of pyruvate with/without mdivi-1 on mitochondrial mean length in cultured MIN6 cells (a) MIN6 cells were prepared as described in supplementary figure 3 and incubated with pyruvate (10 mM) with/without mdivi-1. The untreated low glucose (2 mM) condition served as control. Images were obtained and processed as described in supplementary figure 3. (b) Mean mitochondrial length. Values are given as mean ± SEM (n = 3).

2. Supplementary experimental procedures

a. Human and mouse islet culture conditions

Human islets - Prior to experimentation, human islets (from three different donors) were cultured overnight in Connaught Medical Research Laboratories (CMRL) 1066 medium supplemented

with 10% human serum, 100 units/ml penicillin, 100 μg/ml streptomycin and 2 mM glutamine (Life technologies) at 37°C and 5% CO_2.

	Donar 1	Donar 2	Donar 3
Date of harvesting	November 4 2015 5:15 AM	February 10 2016 11.45 PM	October 25 2016 3.03 AM
Date of processing	November 4 2015 2:01 PM	February 11 2016 11.35 AM	October 25 2016 10.50 AM
Cold ischemic time	06:29	10.25	05:37
Age	65	55	55
Gender	Female	Female	Female
BMI (Kg/m2)	20,8	30,1	24
ABO blood group	O	A	
HLA A	3/19 (31)	02/	2/31(19)
HLA B	7/18	40/	18/44(12)
HLA DR	13/15	13/	15/15
HIV I/II	Negative		Negative
HTLV I/II	Not done		Not done
CMV	Positive		Positive
EBV	Not done		Not done
HBsAg	Negative		Negative
Anti-HBc	Negative		Negative
Cause of death	Trauma		

Mouse islets – Male C57BL/6 mice (Janvier Lab) were housed under a 12-h light-dark cycle with *ad libitum* access to food (chow) and water. Mouse islets were incubated overnight in RPMI 1640 culture medium supplemented with 10% fetal calf serum (Life technologies) at 37°C and 5% CO_2 before experimentation.

b. MIN6 cell culture and viral infection

MIN6 cells - MIN6 cells, a pancreatic mouse insulinoma cell line obtained from Prof. J. Miyazaki (Osaka University, Japan), were maintained in Dulbecco's modified Eagle's medium (DMEM) with glutaMAX containing 25 mM glucose (Life technologies) supplemented with 15% heat-inactivated hyclone serum (Thermo scientific), 72 μM 2-mercaptoethanol (Roth), 100 units/ml penicillin and 100 μg/ml streptomycin (Life Technologies). Cells were incubated at 37°C in a humidified 5% CO_2, 95% air environment. The culture medium was changed every 72 h and passaged when 80-90% confluent.

Viral infection - The pre-made lentiviral pLKO.1 control shRNA and mouse *Drp1* shRNA plasmids were purchased from Sigma. *Drp1* shRNA was used to knockdown the expression of *Drp1* in MIN6 cells. Viral infection was carried out in 96-well plates with 1000 cells/well. After 24 h of culture, cells were infected with shRNA lentiviral particles to give a Multiplicity Of Infection (MOI) of approximately 1. After 24 h of transduction, medium was replaced with selection medium containing 1 μg/ml puromycin. The selection was continued until a stable puromycin-resistant cell population was obtained.

c. Insulin secretion from MIN6 cells

Cells were seeded into 96-well plates at a density of 30,000 cells/well in DMEM containing 25 mM glucose. After 48 h, the standard culture medium was replaced with fresh medium

containing 5 mM glucose for 16 h. The cells were subsequently washed twice with KRH bicarbonate buffer containing 2 mM glucose and starved in the same buffer with and without 25/50 μM mdivi-1 for 2 h. Later, starvation medium was aspirated, and cells were incubated in KRH bicarbonate buffer supplemented with indicated concentrations of glucose and other secretagogues with and without 25/50 μM mdivi-1 for 2 h. The amount of insulin secreted and total insulin content was assayed using the mouse ultrasensitive insulin ELISA kit. DNA content of the cells was measured for normalization. Each independent experiment was performed with four technical replicates.

d. Glucose uptake assay

MIN6 cells were seeded and preincubated, using the same procedure as those employed for determination of insulin secretion. Cells were then incubated with 10 mM glucose and 5 mM 2-deoxyglucose (2-DG) for 2 h. Later, the medium was removed and cells were washed. 2-DG was determined using the calorimetric Glucose Uptake assay kit (Abcam) according to the manufacturer's protocol. Results were corrected for DNA content.

e. Western blot analysis and RNA isolation and RT-PCR

Western blot analysis - Cells were rinsed with ice-cold Dulbecco's PBS and incubated with RIPA lysis buffer containing a cocktail of protease and phosphatase inhibitors. After sonication for 10 sec, cell lysates were centrifuged at 12000 g for 10 min. The protein concentration was determined using a BCA protein assay kit (Thermo scientific) according to the manufacturer's protocol. Protein lysates were prepared in Nu-PAGE LDS sample buffer (Novex). Equal amounts of total cell protein were separated by 10% or 12% sodium dodecyl sulfate polyacrylamide gel electrophoresis (SDS-PAGE) and transferred onto nitrocellulose membrane (Bio-Rad). The membranes were blocked for 1 h in TBS-T containing 5% (w/v) BSA at room

temperature and then probed overnight at 4^0C with appropriate primary antibodies: anti-*Drp1* (BD Bioscience), anti-alpha tubulin (Santa Cruz biotechnology) and anti-actin (Cell signaling). After three washes with TBS-T, membranes were incubated with respective horse peroxidase-conjugated secondary antibodies (Santa Cruz biotechnology) for 1 h in TBS-T containing 5% (w/v) BSA at room temperature. After three washes with TBS-T, the membranes were detected using a chemiluminescence detection system (LI-COR Biosciences). Quantification of band density was performed by densitometric analysis and normalized against alpha tubulin and actin values.

RNA isolation and RT-PCR - At the end of experiment, cells were rinsed with ice-cold Dulbecco's PBS and total RNA was extracted using an RNeasy Mini Kit (Qiagen) according to the manufacturer's instructions. RNA concentration and purity were determined using a Nano drop spectrophotometer (Thermo scientific). cDNA was synthesized from 1 μg of total RNA using a QuantiTect Reverse Transcription Kit (Qiagen) according to the manufacturer's instructions. cDNA was then subjected to real time-PCR using SYBR Green premix (Applied Biosystem). HPRT was used as an internal control. Primers used for real time PCR are listed in Table 1.

f. Primer sequences

Target genes	Forward primer	Reverse primer
DNM1L/ Drp1	TAAGCCCTGAGCCAATCCATC	CATTCCCGGTAAATCCACAAGT
Opa1	TGGAAAATGGTTCGAGAGTCAG	CATTCCGTCTCTAGGTTAAAGCG
Mfn1	CCTACTGCTCCTTCTAACCCA	AGGGACGCCAATCCTGTGA
Mfn2	ACCCCGTTACCACAGAAGAAC	AAAGCCACTTTCATGTGCCTC
INS 1	CACTTCCTACCCCTGCTGG	ACCACAAAGATGCTGTTTGACA
INS 2	GCTTCTTCTACACACCCATGTC	AGCACTGATCTACAATGCCAC
Glut 1	CAGTTCGGCTATAACACTGGTG	GCCCCCGACAGAGAAGATG
Glut 2	TCAGAAGACAAGATCACCGGA	GCTGGTGTGACTGTAAGTGGG
Gck	AACGACCCCTGCTTATCCTC	CTTCTGCATCCGGCTCATCA